Am J Transl Res 2024;16(7):2921-2930
www.ajtr.org /ISSN:1943-8141/AJTR0156750

Original Article

Development and validation of a nomogram incorporating multi-parametric MRI and hematological indicators for discriminating benign from malignant central prostatic nodules: a retrospective analysis

Chunling Xu[1*], Yupeng Zhang[2*], Nailong Jia[2], Chuizhi Huang[2], Qimao Fu[2], Yan Chen[2], Changkun Lin[2]

[1]Department of Imaging, Lianyungang First People's Hospital, Lianyungang 570311, Jiangsu, China; [2]Department of Radiology, The Second Affiliated Hospital of Hainan Medical College, Haikou 570311, Hainan, China. [*]Co-first authors.

Received March 22, 2024; Accepted June 8, 2024; Epub July 15, 2024; Published July 30, 2024

Abstract: Background: Prostate cancer poses a significant risk to men's health. In this study, a model for differentiating benign and malignant nodules in the central region of the prostate was constructed by combining multiparametric MRI and hematological lab values. Methods: This retrospective study analyzed the data acquired from Lianyungang First People's Hospital and The Second Affiliated Hospital of Hainan Medical College from January 2018 to December 2021. We included 310 MRI-confirmed prostatic nodule patients. The data were split into a training set (260 cases) and an external validation set (50 cases), with the latter exclusively from The Second Affiliated Hospital of Hainan Medical College to test the model's generalizability. Univariate and multivariate logistic regression identified critical measurements for differentiating prostate cancer (PCa) from benign prostatic hyperplasia (BPH), which were then integrated into a nomogram model. Results: The key indicators determined by multivariate logistic regression analysis included apparent diffusion coefficient (ADC), standard deviation (StDev), neutrophil to lymphocyte ratio (NLR), and prostate specific antigen (PSA). The nomogram's performance, as indicated by the area under the curve (AUC), was 0.844 (95% CI: 0.811-0.938) in the training set and 0.818 (95% CI: 0.644-0.980) in the external validation set. Calibration and decision curves demonstrated that the nomogram was well-calibrated and could serve as an effective tool in clinical practice. Conclusion: The nomogram model based on ADC, StDev, NLR and PSA may be helpful to identify PCa and BPH.

Keywords: Prostate cancer, nomogram, magnetic resonance imaging, identification

Introduction

Prostate cancer (PCa) is the second most prevalent malignant tumor in men worldwide, following lung cancer [1]. PCa is an age-related disease, typically diagnosed in patients around the age of 66 years [2]. In clinical practice, 30% of PCa cases manifest in the central gland (CG) [3], a region prone to benign prostatic hyperplasia (BPH). Because it presents similarly to BPH in magnetic resonance imaging (MRI) signal characteristics, it can be easily overlooked [4]. Transrectal random transrectal ultrasound is considered the gold standard for diagnosing PCa [5]. However, it is an invasive procedure that frequently leads to complications, including rectal bleeding and hematuria [6]. Prostate-specific antigen (PSA) has traditionally served as a screening tool for PCa, yet its specificity is notably limited. Studies indicate that the specificity of PSA for PCa can be as low as 25% [7], leading to the issue of overdiagnosis. This underscores the urgent need for developing alternative diagnostic methods. Alongside PSA testing, imaging examinations play a crucial role in the diagnosis of PCa, notably MRI with excellent soft component resolution and multi-parameter imaging capabilities. As MRI technology advanc-

https://doi.org/10.62347/RBCM8913

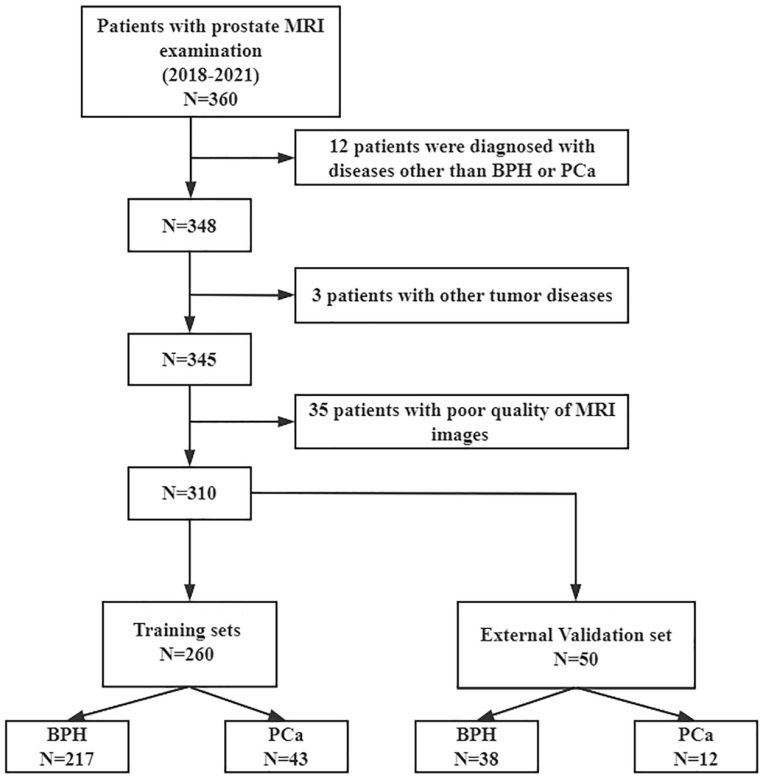

Figure 1. Inclusion and exclusion of patients. MRI, magnetic resonance imaging; Pca, Prostate cancer; BPH, Benign prostatic hyperplasia.

es, multi-sequence imaging techniques such as T2-weighted imaging (T2WI), diffusion-weighted imaging (DWI), and dynamic contrast enhancement (DCE) have emerged. The adoption of multi-parametric MRI (Mp-MRI) has seen rapid progress and use in the field of PCa diagnosis [8].

Yana et al. [9] highlighted that combining PSA with Mp-MRI could enhance diagnostic accuracy. Furthermore, the significance of inflammatory markers in cancer diagnosis and prognosis assessment has garnered increasing attention in recent years. Jethwani et al. [10] proved the predictive value of the neutrophil-to-lymphocyte ratio (NLR) in PCa, while Xu et al. [11] evaluated the effect of monocyte-to-lymphocyte ratio (MLR) in the diagnosis of PCa and found that it may be another good predictor of PCa.

In response to these findings, we developed a nomogram model that integrates Mp-MRI with haematological markers of inflammation to differentiate between PCa and benign prostatic hyperplasia (BPH). This model leverages the precision of MRI and enhances it with inflammatory hematological laboratory values, providing a more holistic approach compared to previous models that may have relied excessively on a single diagnostic marker [12, 13]. By combining Mp-MRI and blood biomarkers, our model aims to significantly improve diagnostic accuracy, which is vital for correctly distinguishing between PCa and BPH.

Materials and methods

Data sources

The data were acquired from the electronic case system of Lianyungang First People's Hospital and the Second Affiliated Hospital of Hainan Medical College from January 2018 to December 2021. A total of 310 patients who underwent MRI examination and were confirmed to have prostate nodules were included in the study. They were divided into a training set (n = 260) and an external verification set (n = 50). The training set was used for the construction and internal verification of the nomograph model, and the verification set was used for the external verification of the model. The external validation set was exclusively sourced from The Second Affiliated Hospital of Hainan Medical College.

Ethics statement

This study was approved by the Medical Ethics Committee of Lianyungang first people's Hospital and The Second Affiliated Hospital of Hainan Medical College. Due to its retrospective nature, written informed consent was exempted since we anonymized all information related to patient privacy.

Inclusion and exclusion criteria

Inclusion Criteria: (i) MRI scans including axial T2WI, DWI and DCE showing a nodular signal in the central area of the prostate; (ii) Diagnosis of BPH or PCa by transrectal ultrasound biopsy within 1-2 weeks following the MRI examination [14].

Table 1. Variance inflation factor values of all independent variables

Variable	VIF
Age (years)	1.101
Ktrans (min^{-1})	1.095
Kep (min^{-1})	1.094
Ve	1.087
FA	1.062
ADC (10^{-3} mm^2/s)	1.082
Entroy	1.098
Meam	1.044
StDev	1.142
Inhomogenity	1.124
Skewness	1.103
Kurtosis	1.068
NLR	1.077
PLR	1.141
MLR	1.081
MPV	1.079
RDW	1.102
PSA (ng/mL)	1.214
fPSA/tPSA	1.087

Ktrans, transport constant; Kep, rate constant; Ve, extravascular extracellular space volume fraction; FA, fractional anisotropy; ADC, apparent diffusion coefficient; StDev, standard deviation; NLR, neutrophil to lymphocyte ratio; PLR, platelet to lymphocyte ratio; MLR, monocyte to lymphocyte ratio; MPV, mean platelet volume; RDW, red blood cell distribution; PSA, prostate specific antigen; tPSA, total prostate specific antigen; fPSA, free prostate specific antigen.

Exclusion Criteria: (i) History of treatment for the prostate disease (such as endocrine therapy, radiation therapy, and chemotherapy) and prior prostate biopsy before the MRI examination; (ii) Presence of other malignancies; (iii) Poor quality of MRI images and incomplete hematological data; (iv) Transrectal ultrasound biopsy diagnosis of PCa concurrent with BPH.

The flow chart details the specific selection process (**Figure 1**).

Data collection

Chunling Xu and Yupeng Zhang collected patient-related data from the hospital's electronic case management system and MIR image storage system, encompassing demographic information such as age, prostate specific antigen (PSA), total prostate specific antigen (tPSA), free prostate specific antigen (fPSA), fPSA/tPSA (f/t), neutrophil to lymphocyte ratio (NLR), platelet to lymphocyte ratio (PLR), monocyte to lymphocyte ratio (MLR), mean platelet volume (MPV), and red blood cell distribution (RDW). Additionally, they collected DCE-MRI imaging parameters, including the volume transport constant (Ktrans), rate constant (Kep), and extravascular extracellular space volume fraction (Ve), as well as DWI-MRI imaging parameters such as fractional anisotropy (FA) and apparent diffusion coefficient (ADC). T2WI-MRI imaging parameters were also included, with texture results characterized by entropy, mean, standard deviation (StDev), inhomogeneity, skewness, and kurtosis. All Mp-MRI texture results were derived from the regions of interest (ROI) delineated using the FireVoxel software (Visual Studio 2019).

Outcome measures

The primary outcome measure was the discriminative ability of the nomogram model for differentiating PCa from BPH, quantified by the receiver operating characteristic (ROC) curve and the area under the curve (AUC). Secondary outcome measures included the model's calibration as assessed by the calibration curve, and its clinical applicability as demonstrated by DCA.

Statistical methods

Texture analysis of T2WI-MRI lesions was conducted using Fire Voxel, while preliminary data screening was performed using SPSS 23.0. Model discrimination was evaluated by the C-index, and internal validation was conducted using 1000 Bootstrap resamples. The DeLong test was used to statistically compare the AUC between groups to ensure the assessment of our model's predictive accuracy. Decision curve analysis (DCA) was used to evaluate the clinical benefit range of the model. A p-value <0.05 was considered significant.

Results

Patient characteristics

Among the 310 subjects included, there were 55 patients with PCa and 255 patients with BPH. They were divided into a training set (PCa group [n = 43]; BPH group [n = 217]) and a validation set (PCa group [n = 12]); BPH group [n =

Table 2. Differences between PCa group and BPH group

Variable	PCa group (n = 43)	BPH group (n = 217)	t value	*P* value
Age (years)	65.51±5.89	64.03±8.33	1.114	0.266
Ktrans (min^{-1})	0.89±0.20	0.81±0.15	2.887	0.004
Kep (min^{-1})	1.10±0.08	1.09±0.04	1.254	0.211
Ve	0.76±0.14	0.75±0.16	0.273	0.785
FA	0.25±0.01	0.25±0.01	1.666	0.097
ADC (10^{-3} mm^2/s)	1.49±0.11	1.56±0.10	4.001	<0.001
Entroy	3.97±0.29	4.01±0.18	1.171	0.243
Meam	105.48±25.45	110.69±30.06	1.064	0.289
StDev	12.59±3.97	17.94±5.21	6.374	0.001
Inhomogenity	0.15±0.03	0.15±0.01	0.921	0.358
Skewness	0.47±0.12	0.50±0.11	1.858	0.064
Kurtosis	1.42±0.35	1.42±0.60	0.079	0.937
NLR	1.73±0.34	1.45±0.24	6.357	<0.001
PLR	157.92±45.56	128.95±35.10	4.690	<0.001
MLR	0.26±0.07	0.25±0.05	1.314	0.190
MPV	11.01±0.89	11.03±0.79	0.161	0.873
RDW	12.79±0.68	12.82±0.58	0.300	0.764
PSA (ng/mL)	8.76±3.94	5.14±1.98	9.000	<0.001
fPSA/tPSA	0.37±0.06	0.39±0.05	1.898	0.059

Ktrans, volume transport constant; Kep, rate constant; Ve, extravascular extracellular space volume fraction; FA, fractional anisotropy; ADC, apparent diffusion coefficient; StDev, standard deviation; NLR, neutrophil to lymphocyte ratio; PLR, platelet to lymphocyte ratio; MLR, monocyte to lymphocyte ratio; MPV, mean platelet volume; RDW, red blood cell distribution; PSA, prostate specific antigen; tPSA, total prostate specific antigen; fPSA, free prostate specific antigen.

38]). After collinearity diagnosis (**Table 1**), the variance inflation factor (VIF) of all variables in this study was less than 10, indicating no significant multicollinearity among the independent variables. There were significant differences in Ktrans, ADC, StDev, NLR, PLR and PSA between the PCa group and BPH group in the training set (**Table 2**). To enhance the clarity for the interpretation of subsequent indicators, we employed the median values from the BPH patients as the threshold for categorizing Ktrans, ADC, StDev, NLR, PLR, and PSA in the multivariate regression analysis, where ADC, StDev, NLR, and PSA were identified as key variables for distinguishing between PCa and BPH (**Table 3**).

Construction of nomogram model

To differentiate between benign and malignant nodules in the central region of the prostate, we constructed a nomogram using ADC, StDev, NLR, and PSA (**Figure 2**). In this model, the total score for each patient is the sum of the scores of each factor. For example, a patient with ADC = 1.5 * 10^{-3} mm^2/s, StDev = 5, NLR = 1.6, PSA = 8 would have scores of 32, 67, 41, 47, respectively for each factor, with a total score of 187 points, and the corresponding probability of PCa would be 0.67 (**Figure 3**).

Additionally, we conducted a comparative analysis to evaluate the predictive efficacy of integrating PSA with MRI-derived imaging metrics and blood laboratory values. This analysis compared the performance of PSA combined with multi-parametric MRI (Mp-MRI) indicators, such as ADC and StDev, against PSA integrated with inflammatory biomarkers like NLR. The comparative findings indicated that a nomogram model, which incorporated ADC, StDev, NLR, and PSA, demonstrated a superior AUC within the training cohort, as detailed in **Table 4**.

Verification of the nomogram model

The internal validation of the nomogram showed an AUC of 0.844 (95% CI: 0.811-0.938), sensitivity of 0.884, and specificity of 0.742, demonstrating robust performance. The C-index was 0.843 (**Figure 4A**), Hosmer-Lemeshow chi-square was 8.343 (*P* = 0.401), and the calibration curve (**Figure 5A**) showed a good agreement between the predicted and observed values of the nomogram. Decision curve analysis (DCA) showed that the model provided clinical benefits in differentiating benign from malignant nodules across a decision threshold range of 10% to 100% (**Figure 6A**).

There was no significant difference in general data between the training group and the validation group (All *P*>0.05, **Table 5**). External validation of the nomogram yielded an AUC of 0.818 (95% CI: 0.644-0.980), sensitivity of 0.750, specificity of 0.941, and C-index of 0.819 (**Figure 4B**). The DeLong test showed that there was no significant difference in AUC between the internal validation and external validation

Table 3. Results of multivariate logistic regression

Variable	*β*	*SE*	*Wald χ2*	*P*	*OR (95% CI)*
Ktrans (min^{-1})					
≤0.80					1
>0.80	0.804	0.410	3.848	0.050	2.234 (1.001-4.988)
ADC (10^{-3} mm^2/s)					
≤1.57					1
>1.57	-0.993	0.444	4.991	0.025	0.371 (0.155-0.885)
StDev					
≤17.78					1
>17.78	1.824	0.498	13.420	<0.001	1.161 (0.061-0.428)
NLR					
≤1.45					1
>1.45	1.449	0.432	11.250	<0.001	4.260 (1.826-9.936)
PLR					
≤127.42					1
>127.42	0.602	0.412	2.135	0.144	1.826 (0.814-4.097)
PSA (ng/mL)					
<5.13					1
>5.13	1.361	0.449	9.190	0.002	3.900 (1.618-9.400)

Ktrans, volume transport constant; StDev, standard deviation; ADC, apparent diffusion coefficient; NLR, neutrophil to lymphocyte ratio; PLR, platelet to lymphocyte ratio; PSA, prostate specific antigen.

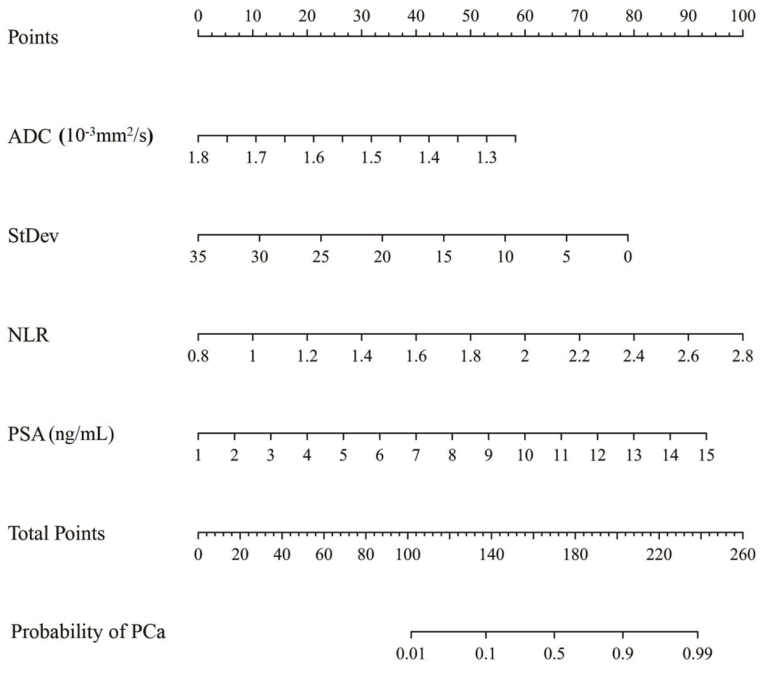

Figure 2. Nomogram model to predict PCa. ADC, apparent diffusion coefficient; StDev, standard deviation; NLR, neutrophil to lymphocyte ratio; PSA, prostate specific antigen; Pca, Prostate cancer.

(Z = 1.322, P = 0.186). The calibration curve (**Figure 5B**) showed good agreement between the predicted and observed values of the nomogram. DCA (**Figure 6B**) was plotted using validation set data and showed that when the threshold probability was 17%-90%, model screening could benefit patients in clinical practice, highlighting the model's practical value in clinical settings.

Discussion

Prostate cancer typically arises from the acinar or ductal epithelium of the prostate gland and often coexists with benign prostatic hyperplasia [15]. Malignancy can develop from benign prostatic nodules. While prostate cancer predominantly originates in the peripheral zone, which is distinct from BPH, a small percentage of cases develop in the central gland where BPH is commonly located [16]. The early clinical symptoms of both PCa and benign BPH often lack specific distinguishing features.

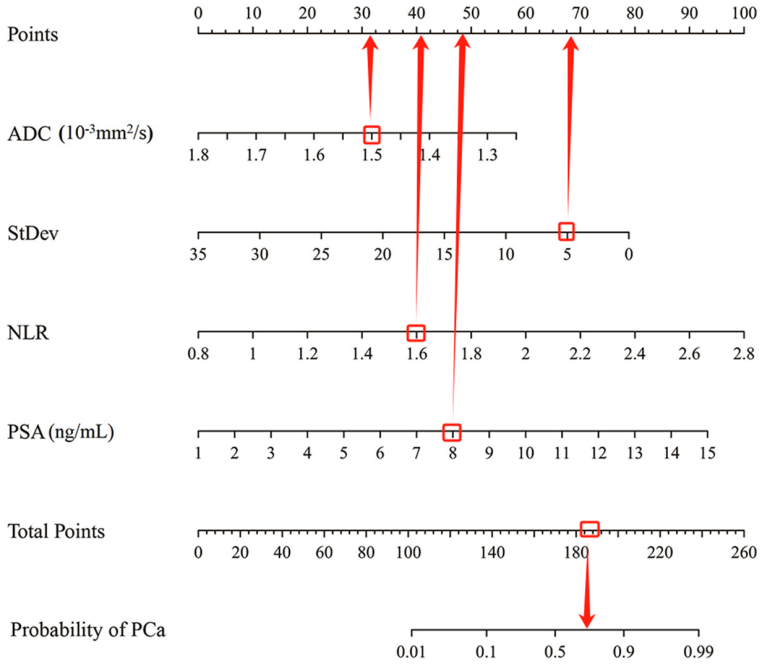

Figure 3. Nomogram model to predict PCa. ADC, apparent diffusion coefficient; StDev, standard deviation; NLR, neutrophil to lymphocyte ratio; PSA, prostate specific antigen; Pca, Prostate cancer.

Table 4. Comparison of the effect of different index modeling on the identification of PCa and BPH in the training set

Model	AUC	*Z*	*P*
ADC+StDev+NLR+PSA	0.884 (0.811-1.938)		
ADC+StDev+PSA	0.842 (0.780-0.903)	1.972[a]	0.049
NLR+PSA	0.821 (0.762-0.890)	2.353[a]	0.019

a, Comparison of AUC with the modeling group based on indicators of ADC, StDev, NLR, and PSA.

By the time noticeable symptoms appear, patients may already be in the intermediate to advanced stages of cancer, missing the optimal window for treatment [17]. Early detection and regular screenings are therefore crucial for timely intervention. The nomogram model proposed in this research could assist healthcare providers in early detection of benign and malignant prostate lesions, enabling effective disease management. Through the analysis of ROC curves, calibration curves, and DCA, it was observed that the nomogram model demonstrated favorable clinical discrimination, accuracy, and clinical utility. By utilizing this nomogram model, medical professionals can predict the likelihood of malignant prostate nodules by calculating the total score based on various factors indicated in the nomogram, facilitating early identification and intervention.

Our study shows that MRI parameters ADC and StDev were influencing factors for malignancy of prostatic nodules. DWI is a non-invasive functional imaging technique that observes the motion of water molecules within living tissues [18]. In the context of prostatic imaging, DWI holds significant utility and can effectively detect early lesions, contributing to the early diagnosis and management of prostate conditions [19]. ADC value serves as a quantitative measure indicative of the diffusion capacity of water molecules in DWI [15]. In PCa patients, the densely packed and proliferating cancer cells lead to restricted intercellular spaces, impeding the diffusion of water molecules and consequently resulting in decreased ADC values [21]. In contrast, although BPH also involves cell proliferation, it primarily affects the growth of interstitial components such as fibroblasts, with minimal changes in prostate cell volume, contributing to a relatively stable ADC value alteration [22]. Research indicates that the combination of DWI with ADC can achieve high specificity and sensitivity for diagnosing PCa [23]. While T2WI offers superior resolution for depicting the anatomic structure of the prostate compared to DWI [24], both PCa and BPH exhibit low signal intensities on T2WI images, leading to challenges in differential identification [25]. By utilizing histogram analysis, texture features from T2WI images can be extracted, aiding in the differentiation of PCa from other prostate conditions [26]. In this study, the software Fire Voxel was employed to extract five texture quantitative parameters from the images, with only StDev showing statistical differences between the groups. StDev denotes the variation in signal intensity within the tissue [27]. When tumor tissue hyperplasia

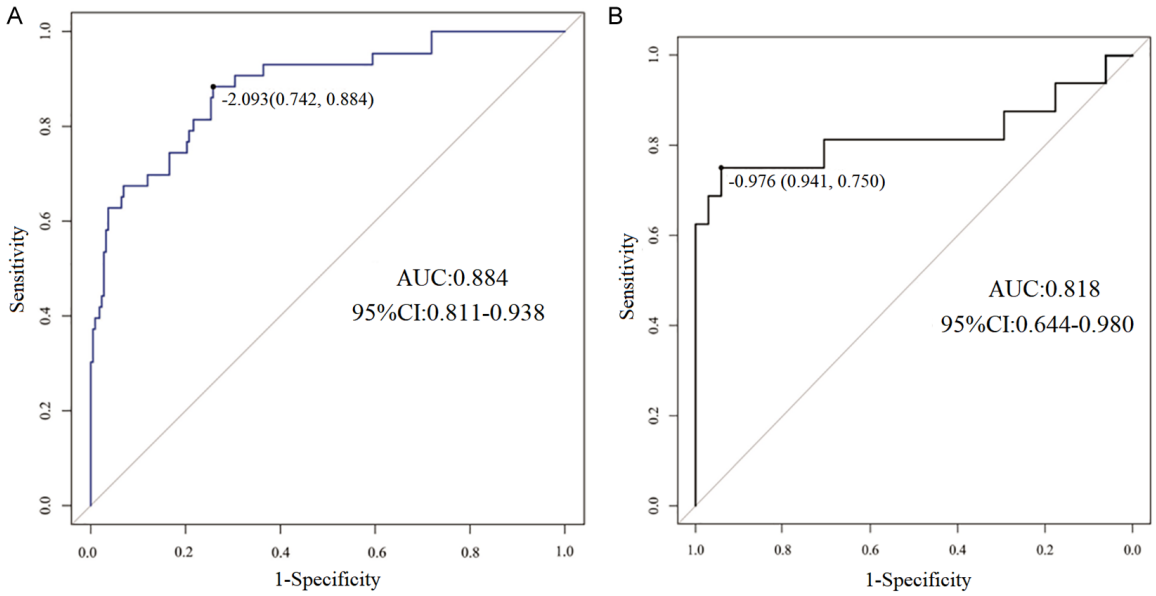

Figure 4. ROC curve of the model in internal validation and external validation. A. Internal validation; B. External validation.

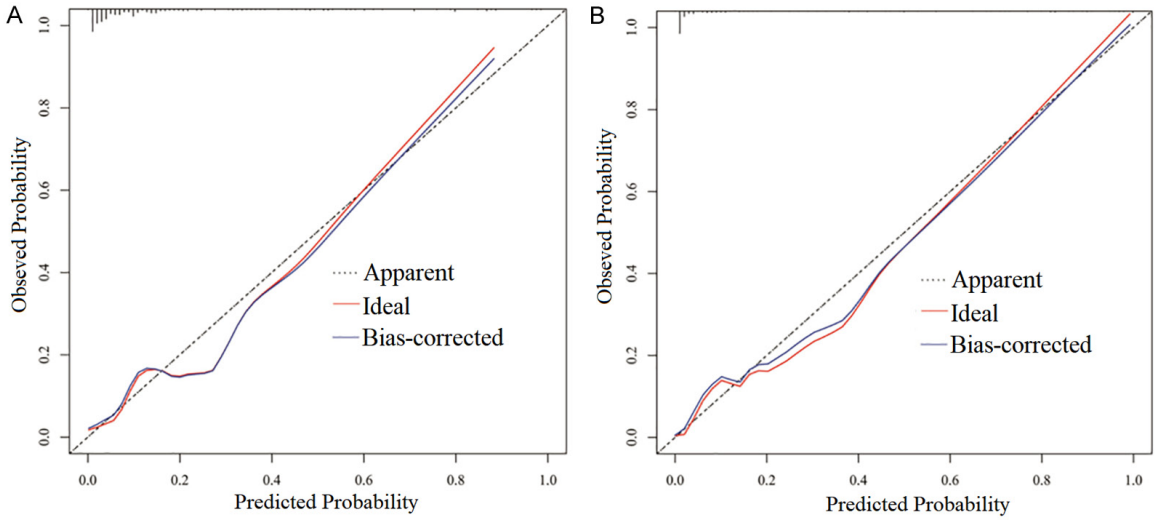

Figure 5. Calibration curves of the model in internal validation and external validation. A. Internal validation; B. External validation.

replaces the original structures like glands, stroma, and blood vessels, forming irregular or patchy tumor parenchyma, it diminishes the morphologic diversity of tissue structure, thereby resulting in a smaller StDev value than that of proliferative tissue.

Many studies have confirmed the role of inflammation in tumors, including NSCLC [28], colon cancer [29], and breast cancer [30]. Adhyatma et al. showed that NLR and PLR may be predictors of PCa [31]. Espinoza et al. found that PCa patients had higher NLR and PLR than BPH patients [32]. We also found that NLR and PLR were significantly different between the two groups. Through multivariate logistic regression, we found that NLR, rather than PLR, was an influencing factor for PCa, which may be related to the difference in patient data we included. PSA, a tissue-specific single-chain polypeptide secreted by prostate acinar and ductal epithelial cells [33], was approved by the

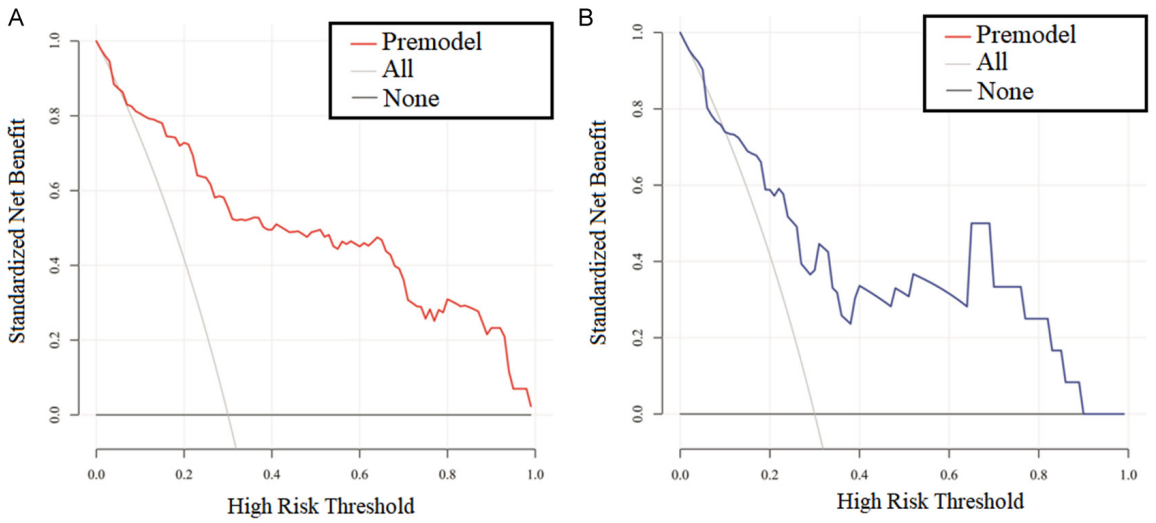

Figure 6. DCA of the model in internal validation and external validation. A. Internal validation; B. External validation.

Table 5. Comparison of data between training group and validation group

Variable	Training sets (n = 260)	External Validation set (n = 50)	t value	*P* value
Age (years)	64.27±7.98	65.26±7.44	0.809	0.419
Ktrans (min^{-1})	0.82±0.16	0.81±015	0.569	0.570
Kep (min^{-1})	1.09±0.05	1.09±0.05	0.177	0.859
Ve	0.75±0.16	0.75±0.14	0.077	0.939
FA	0.25±0.01	0.25±0.01	1.747	0.082
ADC (10^{-3} mm^2/s)	1.55±0.10	1.55±0.11	0.056	0.956
Entroy	4.01±0.20	4.00±0.20	1.551	0.122
Meam	109.83±29.37	107.72±32.40	0.457	0.648
StDev	17.05±5.40	16.51±4.88	0.658	0.511
Inhomogenity	0.15±0.02	0.15±0.02	1.134	0.258
Skewness	0.49±0.11	0.52±0.10	1.487	0.138
Kurtosis	1.42±0.57	1.50±0.66	0.133	0.894
NLR	1.50±0.28	1.57±0.29	1.644	0.101
PLR	133.74±38.48	131.62±31.99	0.365	0.715
MLR	0.25±0.05	0.26±0.06	0.835	0.404
MPV	11.02±0.81	11.10±0.82	0.573	0.567
RDW	12.81±0.60	12.89±0.56	0.896	0.371
PSA (ng/mL)	5.74±2.76	5.38±2.32	0.875	0.382
fPSA/tPSA	0.39±0.05	0.39±0.05	0.062	0.951

Ktrans, volume transport constant; Kep, rate constant; Ve, extravascular extracellular space volume fraction; FA, fractional anisotropy; ADC, apparent diffusion coefficient; StDev, standard deviation; NLR, neutrophil to lymphocyte ratio; PLR, platelet to lymphocyte ratio; MLR, monocyte to lymphocyte ratio; MPV, mean platelet volume; RDW, red blood cell distribution; PSA, prostate specific antigen; tPSA, total prostate specific antigen; fPSA, free prostate specific antigen.

US Food and Drug Administration (FDA) for the detection of PCa in 1986, with PSA<4 ng/mL considered normal [34]. However, later studies have revealed that the specificity of PSA screening based on this threshold is very low, leading to a high false-positive rate and potential misdiagnoses. Therefore, PSA in the range of 4-10 ng/mL is now considered to be a gray area, necessitating additional markers for accurate identification. Our study developed a nomogram that combines PSA with other indicators including ADC, StDev, and NLR to distinguish PCa from BPH, and achieved good discrimination. The verification results of the model showed that the AUC was 0.844, the sensitivity and specificity were 0.844, and 0.724, respectively. Compared to the internal validation, the AUC (0.818) and sensitivity (0.750) of the model in the external validation decreased slightly, and the specificity (0.941) increased slightly, but the overall difference was not significant, affirming the model's robustness and reliability across different patient populations.

However, this study has limitations. As a retrospective analysis, there is an inherent risk of selection bias. Additionally, the external valida-

tion set, despite being from a different hospital, had a smaller sample size, which may contribute to a wider confidence interval observed for the AUC value. The disparity in sample sizes between the PCa and BPH groups could also affect the model's robustness. To address these issues, future research needs to employ a prospective design with larger and more diverse cohorts to enhance the model's external validity and confirm our findings.

Conclusions

The nomogram model based on ADC, StDev, NLR and PSA demonstrates utility in distinguishing PCa from BPH. This tool offers a promising approach for improving diagnostic accuracy and could significantly aid in the early identification and appropriate management of these conditions.

Disclosure of conflict of interest

None.

Address correspondence to: Nailong Jia, Department of Radiology, The Second Affiliated Hospital of Hainan Medical College, Haikou 570311, Hainan, China. Tel: +86-0898-66809032; E-mail: dbhui013@hainmc.edu.cn

References

[1] Moch H, Cubilla AL, Humphrey PA, Reuter VE and Ulbright TM. The 2016 WHO classification of tumours of the urinary system and male genital organs-part A: renal, penile, and testicular tumours. Eur Urol 2016; 70: 93-105.

[2] Panigrahi GK, Praharaj PP, Kittaka H, Mridha AR, Black OM, Singh R, Mercer R, van Bokhoven A, Torkko KC, Agarwal C, Agarwal R, Abd Elmageed ZY, Yadav H, Mishra SK and Deep G. Exosome proteomic analyses identify inflammatory phenotype and novel biomarkers in African American prostate cancer patients. Cancer Med 2019; 8: 1110-1123.

[3] Jemal A, Bray F, Center MM, Ferlay J, Ward E and Forman D. Global cancer statistics. CA Cancer J Clin 2011; 61: 69-90.

[4] Pinto F, Totaro A, Calarco A, Sacco E, Volpe A, Racioppi M, D'Addessi A, Gulino G and Bassi P. Imaging in prostate cancer diagnosis: present role and future perspectives. Urol Int 2011; 86: 373-382.

[5] Hodge KK, McNeal JE, Terris MK and Stamey TA. Random systematic versus directed ultrasound guided transrectal core biopsies of the prostate. J Urol 1989; 142: 71-74; discussion 74-75.

[6] Graif T, Loeb S, Roehl KA, Gashti SN, Griffin C, Yu X and Catalona WJ. Under diagnosis and over diagnosis of prostate cancer. J Urol 2007; 178: 88-92.

[7] Mistry K and Cable G. Meta-analysis of prostate-specific antigen and digital rectal examination as screening tests for prostate carcinoma. J Am Board Fam Pract 2003; 16: 95-101.

[8] Tang JE, Zheng XY, Wang X, Xie LP, Wang RJ, Chen Y and Gao JG. Application of artificial intelligence combined with multi-parametric MRI in the early diagnosis of prostate cancer. Zhonghua Nan Ke Xue 2020; 26: 783-787.

[9] Yanai Y, Kosaka T, Hongo H, Matsumoto K, Shinojima T, Kikuchi E, Miyajima A, Mizuno R, Mikami S, Jinzaki M and Oya M. Evaluation of prostate-specific antigen density in the diagnosis of prostate cancer combined with magnetic resonance imaging before biopsy in men aged 70 years and older with elevated PSA. Mol Clin Oncol 2018; 9: 656-660.

[10] Jethwani DL, Sivamoorthy LL, Toh CC and Malek R. Predicting the diagnosis of prostate cancer with a scoring system based on novel biomarkers. BMC Urol 2022; 22: 13.

[11] Xu Z, Zhang J, Zhong Y, Mai Y, Huang D, Wei W, Huang J, Zhao P, Lin F and Jin J. Predictive value of the monocyte-to-lymphocyte ratio in the diagnosis of prostate cancer. Medicine (Baltimore) 2021; 100: e27244.

[12] Radtke JP, Wiesenfarth M, Kesch C, Freitag MT, Alt CD, Celik K, Distler F, Roth W, Wieczorek K, Stock C, Duensing S, Roethke MC, Teber D, Schlemmer HP, Hohenfellner M, Bonekamp D and Hadaschik BA. Combined clinical parameters and multiparametric magnetic resonance imaging for advanced risk modeling of prostate cancer-patient-tailored risk stratification can reduce unnecessary biopsies. Eur Urol 2017; 72: 888-896.

[13] Dickinson L, Ahmed HU, Hindley RG, McCartan N, Freeman A, Allen C, Emberton M and Kirkham AP. Prostate-specific antigen vs. magnetic resonance imaging parameters for assessing oncological outcomes after high intensity-focused ultrasound focal therapy for localized prostate cancer. Urol Oncol 2017; 35: 30.e39-30.e15.

[14] Hoffman RM. Clinical practice. Screening for prostate cancer. N Engl J Med 2011; 365: 2013-2019.

[15] Gandaglia G, Leni R, Bray F, Fleshner N, Freedland SJ, Kibel A, Stattin P, Van Poppel H and La Vecchia C. Epidemiology and prevention of prostate cancer. Eur Urol Oncol 2021; 4: 877-892.

[16] Engelbrecht MR, Huisman HJ, Laheij RJ, Jager GJ, van Leenders GJ, Hulsbergen-Van De Kaa CA, de la Rosette JJ, Blickman JG and Barentsz JO. Discrimination of prostate cancer from normal peripheral zone and central gland tissue by using dynamic contrast-enhanced MR imaging. Radiology 2003; 229: 248-254.
[17] Rawla P. Epidemiology of prostate cancer. World J Oncol 2019; 10: 63-89.
[18] Bammer R. Basic principles of diffusion-weighted imaging. Eur J Radiol 2003; 45: 169-184.
[19] Tamada T, Ueda Y, Ueno Y, Kojima Y, Kido A and Yamamoto A. Diffusion-weighted imaging in prostate cancer. MAGMA 2022; 35: 533-547.
[20] Cao M, Wang X, Liu F, Xue K, Dai Y and Zhou Y. A three-component multi-b-value diffusion-weighted imaging might be a useful biomarker for detecting microstructural features in gliomas with differences in malignancy and IDH-1 mutation status. Eur Radiol 2023; 33: 2871-2880.
[21] Giganti F, Pecoraro M, Fierro D, Campa R, Del Giudice F, Punwani S, Kirkham A, Allen C, Emberton M, Catalano C, Moore CM and Panebianco V. DWI and PRECISE criteria in men on active surveillance for prostate cancer: a multicentre preliminary experience of different ADC calculations. Magn Reson Imaging 2020; 67: 50-58.
[22] Zhang JW, Liu JJ, Huang T, Zhao YY, Cai L and Chen ZQ. Multi-modality MRI parameters correlate with the expression of the P504s protein in prostate cancer. Zhonghua Nan Ke Xue 2019; 25: 619-625.
[23] Zhou H, Hallac RR, Yuan Q, Ding Y, Zhang Z, Xie XJ, Francis F, Roehrborn CG, Sims RD, Costa DN, Raj GV and Mason RP. Incorporating oxygen-enhanced MRI into multi-parametric assessment of human prostate cancer. Diagnostics (Basel) 2017; 7: 48.
[24] Wu LM, Xu JR, Ye YQ, Lu Q and Hu JN. The clinical value of diffusion-weighted imaging in combination with T2-weighted imaging in diagnosing prostate carcinoma: a systematic review and meta-analysis. AJR Am J Roentgenol 2012; 199: 103-110.
[25] Xing P, Chen L, Yang Q, Song T, Ma C, Grimm R, Fu C, Wang T, Peng W and Lu J. Differentiating prostate cancer from benign prostatic hyperplasia using whole-lesion histogram and texture analysis of diffusion- and T2-weighted imaging. Cancer Imaging 2021; 21: 54.
[26] Ma L, Zhou Q, Yin H, Ang X, Li Y, Xie G and Li G. Texture analysis based on PI-RADS 4/5-scored magnetic resonance images combined with machine learning to distinguish benign lesions from prostate cancer. Transl Cancer Res 2022; 11: 1146-1161.
[27] Wibmer A, Hricak H, Gondo T, Matsumoto K, Veeraraghavan H, Fehr D, Zheng J, Goldman D, Moskowitz C, Fine SW, Reuter VE, Eastham J, Sala E and Vargas HA. Haralick texture analysis of prostate MRI: utility for differentiating non-cancerous prostate from prostate cancer and differentiating prostate cancers with different Gleason scores. Eur Radiol 2015; 25: 2840-2850.
[28] Liu S, Zhao L and Zhou G. Peripheral blood markers predict immunotherapeutic efficacy in patients with advanced non-small cell lung cancer: a multicenter study. Front Genet 2022; 13: 1016085.
[29] Polk N, Budai B, Hitre E, Patocs A and Mersich T. Corrigendum: high neutrophil-to-lymphocyte ratio (NLR) and systemic immune-inflammation index (SII) are markers of longer survival after metastasectomy of patients with liver-only metastasis of rectal cancer. Pathol Oncol Res 2022; 28: 1610658.
[30] Jalali A, Miresse D, Fahey MR, Ni Mhaonaigh N, McGuire A, Bourke E, Kerin MJ and Brown JAL. Peripheral blood cell ratios as prognostic indicators in a neoadjuvant chemotherapy-treated breast cancer cohort. Curr Oncol 2022; 29: 7512-7523.
[31] Adhyatma KP and Warli SM. Diagnostic value of platelet-to-lymphocyte ratio in prostate cancer. Open Access Maced J Med Sci 2019; 7: 1093-1096.
[32] Espinoza AR, Lavi J, Otano N, Arenilla W, Leon R, Espinoza A, Salvador N and Leon A. Serum cellular inflammatory markers in the diagnosis of prostate cancer. Arch Esp Urol 2019; 72: 641-646.
[33] Bevacqua E, Ammirato S, Cione E, Curcio R, Dolce V and Tucci P. The potential of microRNAs as non-invasive prostate cancer biomarkers: a systematic literature review based on a machine learning approach. Cancers (Basel) 2022; 14: 5418.
[34] Merriel SWD, Pocock L, Gilbert E, Creavin S, Walter FM, Spencer A and Hamilton W. Systematic review and meta-analysis of the diagnostic accuracy of prostate-specific antigen (PSA) for the detection of prostate cancer in symptomatic patients. BMC Med 2022; 20: 54.